**ORIGINAL ARTICLE**

# Mathematical analysis of the flow and heat transfer of Ag-Cu hybrid nanofluid over a stretching/shrinking surface with convective boundary condition and viscous dissipation

R. Jusoh[1,*], K. Naganthran[2], A. Jamaludin[3], M.H. Ariff[4], M.F.M Basir[5] and I. Pop[6]

[1]Centre for Mathematical Sciences, College of Computing and Applied Sciences, Universiti Malaysia Pahang, Lebuhraya Tun Razak, 26300 Gambang, Kuantan, Pahang, Malaysia.
[2]Department of Mathematical Sciences, Faculty of Science and Technology, Universiti Kebangsaan Malaysia, Bangi 43600, Selangor, Malaysia.
[3]Department of Mathematics, Universiti Pertahanan Nasional Malaysia, 57000 Kuala Lumpur, Malaysia.
[4]Faculty of Electrical & Electronics Engineering Technology, Universiti Malaysia Pahang, 26600 Pekan, Pahang, Malaysia.
[5]Department of Mathematical Sciences, Faculty of Science, Universiti Teknologi Malaysia, UTM, 81310 Johor Bahru, Malaysia.
[6]Department of Mathematics, Babeş-Bolyai University, R-400084 Cluj-Napoca, Romania.

**ABSTRACT** – Hybrid nanofluid has a vast potential of applications in the cooling system due to the high thermal conductivity. This study emphasizes on the impact of the convective boundary condition and viscous dissipation to the heat transfer of Ag-Cu hybrid nanofluid. A suitable similarity transformation is used to transform the partial differential equations of mass, momentum and energy into the ordinary differential equations. A finite difference code known as bvp4c in Matlab is employed to generate the numerical solutions. Stability analysis is conducted since dual solutions are generated in this study and the first solution exhibits the stability properties. The influence of variations in the suction parameter, viscous dissipation, nanoparticles concentration and Biot number on the on the temperature and velocity profiles of the hybrid nanofluid are portrayed. The rate of heat transfer is prominently higher with the augmentation of the Biot number and Ag nanoparticles concentration.

## INTRODUCTION

Since decades ago, researchers and scientists have explored various methodologies and techniques to boost the heat transfer capability of fluid. The intensified coolant has been an urgent need nowadays to support the advance technological appliances, transportation system and diverse industries. This led to the discovery of nanofluids which are the fluids that contain nano sized solid particles by Choi and Eastman [1]. They found that nanofluids exhibit higher thermal conductivity then the conventional fluids. Afterwards, thriving research was done to investigate the mechanisms of heat transfer in nanofluids. Saidur et al. [2] reported that heat transfer process in nanofluid is more promising since it has higher dispersion stability and wider surface area between fluids and nanoparticles. In the cooling system of an electronic liquid, Nguyen et al. [3] experimentally proved that the heat transfer coefficient for $Al_2O_3$-water nanofluid increased 40% with 6.8% volume fraction nanoparticles. Khoshvaght-Aliabadi and Alizadeh [4] conducted an experiment of Cu-water nanofluid flow inside serpentine tubes. and found that the thermal–hydraulic performance of the serpentine tubes enhanced about 10%. Later, Koca et al. [5] scrutinized the performance of Ag-water nanofluid in the single phase circulation loop. An outstanding result had been obtained with 1% concentration of Ag nanoparticles where the effectiveness of the heat transfer is increased up to 11%. This specialty of nanofluid contributes to the plentiful applications such as in the microchips cooling system, thermal energy storage, optical devices, delivery of transdermal drug, geothermal power extraction, cancer therapeutics, braking system, solar collectors, automotive lubrication, sensing and imaging system, nuclear reactor, nanocryosurgery and heat exchanging fluid system [6]–[9]. Besides, researchers also analyzed the properties of nanofluid mathematically and provided some meaningful numerical results by using the shooting method, homotopy analysis method and Keller box method [10]–[16].

Nowadays, researchers extending the potential of nanofluids by considering two different types of nanoparticles suspension in the base fluid. Specifically, this new type of fluid is called as hybrid nanofluid. The nanoparticles are including the carbon nanotubes (CNT), stable metals like silver (Ag) and copper (Cu), and metal oxides such as ZnO, $TiO_2$, $SiO_2$, $Al_2O_3$ and $Fe_3O_4$ [17]. The invention of utilizing hybrid nanofluids is to enhance the heat transfer capability of the single type nanoparticle fluid. Devi and Devi [18] found that with the existence of magnetic field, the rate of heat transfer involving Cu-Al2O3/water hybrid nanofluid is higher than Cu/water nanofluid. After that, Minea [19] studied the hybrid nanofluids based on $TiO_2$, $SiO_2$ and $SiO_2$ and discovered at least 12% increment of thermal conductivity with nanoparticles addition. Radiation and slip effects on the rotating flow of Ag-Cuo/water hybrid nanofluid had been studied by Hayat et al. [20]. They noticed that rotation and radiation increased the hybrid nanofluids temperature. Other than that,

researchers also consider various types of physical parameters and flow configuration of hybrid nanofluids to explore their full heat transfer potential [21]–[26]. Recently, an interesting finding has been obtained by Chahregh and Dinarvand [27] where they found that $TiO_2$-Ag/blood hybrid nanofluid can be a promising medium for drug delivery in the respiratory system.

One of the physical parameter that captivates the researchers' attention is the viscous dissipation effect since it is related to some physical phenomena. For instance, in the polymer processing flows and aerodynamic heating where the viscous dissipation is significant in enhancing the surface temperature [28], [29]. Bataller [30] stated that the inclusion of viscous dissipation in the energy equation is vital due to the importance of temperature distribution ascertainment in the unavoidable internal friction condition. Usually, this situation occurs in the bio-engineering industry, chemical and food processing and oil-exploitation. Mabood et al. [31] explained that the element of viscous stress drives the viscous dissipation to act as an internal heat source and consequently boosts the dimensionless temperature. Numerous articles flooded the field of boundary layer flow with viscous dissipation impact [30–33]. Currently, Lund et al. [36] considered viscous dissipation in the flow of Cu-$Al_2O_3$/$H_2O$ hybrid nanofluid over a shrinking surface. They concluded that the temperature profiles increase with the increment in viscous dissipation.

In addition, convective boundary condition also part of the interest in the boundary layer flow research. Sometimes, it is also known as the Robin condition. Physically, it can be described as a condition where the heat conduction at the surface equals to the heat convection. Heat exchange performance is affected by the interaction between the thermal boundary layer formation in the hot fluid and the axial wall conduction. Convective heat transfers also involve in procedures with high temperature. Such situation arise in the nuclear plant, hemodialysis, oxygenation, laser therapy, sanitary fluid transport, gas turbines and material drying [37], [38]. Ibrahim and Ul-Haq [39] considered convective boundary condition in the stagnation point flow of nanofluid. They concluded that the higher convection which represented by the higher Biot number contributed to the enhancement of heat transfer. The same result was obtained by Rosali et al. [40] where they found a rise in the values of Nusselt number with an increment in the convective heat transfer parameter. Furthermore, several researchers also analyzed the impact of convective boundary condition to the process of heat exchange in hybrid nanofluids [41]–[43].

The aforementioned researches motivate the authors to investigate the coupling influence of viscous dissipation and convective boundary condition to the Ag-Cu hybrid nanofluid. Combination of Ag and Cu nanoparticles are chosen in this study because these nanoparticles have high thermal conductivity. In addition, these nanoparticles also had been proven give more improvements on the Nusselt number scientifically [44]. Besides using water, we also generate the temperature profile for Ag-Cu hybrid nanofluid with methanol and kerosene as the base fluid. We have solved the mathematical model of Ag-Cu hybrid nanofluid numerically and presented dual solutions for some values of the governing parameters. Stability analysis also has been conducted to intent on which solution is stable. It is worth mentioning that this study is purely original and the numerical results have never been published by any other researchers before. The presented mathematical analysis and numerical results will contribute to the further understanding of the heat transfer mechanism in hybrid nanofluids.

## MATHEMATICAL FORMULATION

A steady two dimensional Ag-Cu hybrid nanofluid flow is considered in this study. Figure 1 shows the physical configuration of the hybrid nanofluid flow. The surface is positioned at $y = 0$ and permeably stretched/shrunk in $x$-axis with the velocity $u = \lambda u_w(x) = \lambda ax$ where specifically, $a$ is a constant and $\lambda < 0$ describes the shrinking sheet while the stretching sheet is defined by $\lambda > 0$. The mass flux velocity is assumed as $v = v_w$. Besides, convective boundary condition also has been considered in this model where the hot fluid of uniform temperature $T_f$ with the heat transfer coefficient $h_f$ is heating up the surface convectively and $T_\infty$ represents the ambient fluid temperature.



(a) The sheet is stretched $(\lambda > 0)$      (b) The sheet is shrunk $(\lambda < 0)$
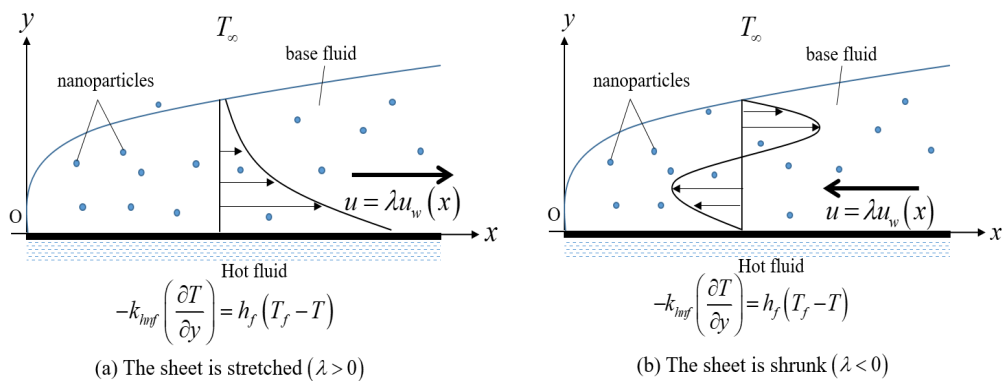
**Figure 1.** Physical diagram of the hybrid nanofluid flow over the stretching/shrinking surface with convective boundary condition.

By complying the above mentioned assumptions, the governing boundary layer flow equations for Ag-Cu hybrid nanofluid are specified as follows:

$$\frac{\partial u}{\partial x} + \frac{\partial v}{\partial y} = 0, \tag{1}$$

$$u\frac{\partial u}{\partial x} + v\frac{\partial u}{\partial y} = \frac{\mu_{hnf}}{\rho_{hnf}}\frac{\partial^2 u}{\partial y^2}, \tag{2}$$

$$u\frac{\partial T}{\partial x} + v\frac{\partial T}{\partial y} = \alpha_{hnf}\frac{\partial^2 T}{\partial y^2} + \frac{\mu_{hnf}}{(\rho C_p)_{hnf}}\left(\frac{\partial u}{\partial y}\right)^2, \tag{3}$$

and depending on the boundary conditions

$$u = \lambda u_w(x) = \lambda ax, \quad v = v_w, \quad -k_{hnf}\left(\frac{\partial T}{\partial y}\right) = h_f\left(T_f - T\right) \quad \text{at} \quad y = 0,$$

$$u \to 0, \quad T \to T_\infty \quad \text{as} \quad y \to \infty. \tag{4}$$

where $u$ is the velocity component in $x$ direction whereas $v$ is the velocity component in $y$ direction and the hybrid nanofluid temperature is denoted by $T$., The other parameters for hybrid nanofluid are the dynamic viscosity, density, thermal diffusivity, thermal conductivity and heat capacity which represented by $\mu_{hnf}$, $\rho_{hnf}$, $\alpha_{hnf}$, $k_{hnf}$ and $(\rho C_p)_{hnf}$, respectively. The formula of the thermophysical properties for hybrid nanofluid are provided in Table 1. In this table, subscript $s1$ and $s2$ are used to represent two different types of nanoparticles, $f$ for the base fluid, $nf$ for nanofluid and $hnf$ for hybrid nanofluid. Table 2 provides the values of thermophysical properties for the nanoparticles (Ag and Cu) while Table 3 for the base fluids (water, methanol and kerosene).

**Table 1.** Formula of thermophysical properties for nanofluid and hybrid nanofluid.

| Properties | Nanofluid | Hybrid nanofluid |
|---|---|---|
| Density | $\rho_{nf} = (1-\phi_1)\rho_f + \phi_1\rho_s$ | $\rho_{hnf} = (1-\phi_2)\left[(1-\phi_1)\rho_f + \phi_1\rho_{s1}\right] + \phi_2\rho_{s2}$ |
| Heat capasity | $(\rho C_p)_{nf} = (1-\phi_1)(\rho C_p)_f + \phi_1(\rho C_p)_{s1}$ | $(\rho C_p)_{hnf} = (1-\phi_2)\begin{bmatrix}(1-\phi_1)(\rho C_p)_f \\ +\phi_1(\rho C_p)_{s1}\end{bmatrix} + \phi_2(\rho C_p)_{s2}$ |
| Dynamic viscosity | $\mu_{nf} = \dfrac{\mu_f}{(1-\phi_1)^{2.5}}$ | $\mu_{hnf} = \dfrac{\mu_f}{(1-\phi_1)^{2.5}(1-\phi_2)^{2.5}}$ |
| Thermal Conductivity | $k_{nf} = \dfrac{k_{s1} + 2k_f - 2\phi_1(k_f - k_{s1})}{k_{s1} + 2k_f + \phi_1(k_f - k_{s1})} \times k_f$ | $k_{hnf} = \dfrac{k_{s2} + 2k_{nf} - 2\phi_2(k_{nf} - k_{s2})}{k_{s2} + 2k_{nf} + \phi_2(k_{nf} - k_{s2})} \times k_{nf}$ where $\\ k_{nf} = \dfrac{k_{s1} + 2k_f - 2\phi_1(k_f - k_{s1})}{k_{s1} + 2k_f + \phi_1(k_f - k_{s1})} \times k_f$ |

**Table 2.** Thermophysical properties of the nanoparticles. [45][46]

| Properties | $\rho\left(kgm^{-3}\right)$ | $C_p\left(Jkg^{-1}K^{-1}\right)$ | $k\left(Wm^{-1}K^{-1}\right)$ |
|---|---|---|---|
| Cu (Copper) | 8933 | 385 | 401 |
| Ag (Silver) | 10500 | 235 | 429 |

**Table 3.** Thermophysical properties of the base fluids. [47][48]

| Properties | Water ($H_2O$) | Methanol | Kerosene |
|---|---|---|---|
| $\rho\left(kgm^{-3}\right)$ | 997.1 | 792 | 783 |
| $C_p\left(Jkg^{-1}K^{-1}\right)$ | 4179 | 2545 | 2090 |
| $k\left(Wm^{-1}K^{-1}\right)$ | 0.613 | 0.2035 | 0.15 |
| Pr | 6.2 | 7.38 | 21 |

Further, the following similarity transformations are employed to solve Eqs. (1) – (3) together with boundary condition (4):

$$\eta = y\sqrt{\frac{a}{v_f}}, \qquad u = axf'(\eta), \qquad v = -\sqrt{av_f}\,f(\eta), \qquad \theta(\eta) = \frac{T - T_\infty}{T_f - T_\infty}. \tag{5}$$

where the prime signifies differentiation with respect to $\eta$. Then, the replacement of the above similarity transformation yields the following ordinary differential equations:

$$\frac{\mu_{hnf}/\mu_f}{\rho_{hnf}/\rho_f}f''' + ff'' - f'^2 = 0, \tag{6}$$

$$\frac{k_{hnf}/k_f}{\Pr(\rho C_p)_{hnf}/(\rho C_p)_f}\theta'' + f\theta' + \frac{Ec}{[(1-\phi_1)^{2.5}(1-\phi_2)^{2.5}(\rho C_p)_{hnf}]/(\rho C_p)_f}f''^2 = 0, \tag{7}$$

and the boundary conditions turn into

$$f(0) = s, \quad f'(0) = \lambda, \quad \theta'(0) = -\frac{k_f}{k_{hnf}}\Gamma\left(1 - \theta(0)\right), \tag{8}$$

$$f'(\eta) \to 0, \quad \theta(\eta) \to 0 \quad \text{as} \quad \eta \to \infty.$$

where $\Pr = \dfrac{v_f}{\alpha_f}$ is Prandtl number and $Ec = \dfrac{u_w^{\,2}}{(C_p)_f(T_w - T_\infty)}$ is Eckert number which characterizes the viscous dissipation. In addition, $s = -\dfrac{v_w}{\sqrt{av_f}}$ denotes the mass flux parameter where the positive value of $s$ is representing the suction while the negative value of $s$ is demonstrating injection. Another parameter is Biot number which can be defined as $\Gamma = \dfrac{h_f}{k_f}\sqrt{\dfrac{v_f}{a}}$. In this study, the attentive physical quantities are the skin friction coefficient $C_f$ and the Nusselt number $Nu_x$. These parameters can be specified as follows:

$$C_f = \frac{\mu_{hnf}\left(\frac{\partial u}{\partial y}\right)_{y=0}}{\rho_f u_w^{\,2}}, \qquad Nu_x = -\frac{xk_{hnf}\left(\frac{\partial T}{\partial y}\right)_{y=0}}{k_f(T_w - T_\infty)}. \tag{9}$$

Applying the similarity transformation (5), we get

$$C_f \operatorname{Re}_x^{1/2} = \frac{f''(0)}{(1-\phi_1)^{2.5}(1-\phi_2)^{2.5}}, \qquad Nu_x \operatorname{Re}_x^{-1/2} = -\frac{k_{hnf}}{k_f}\theta'(0). \tag{10}$$

where $\operatorname{Re}_x = xu_w/v_f$ is the local Reynolds number

## STABILITY ANALYSIS

Apparently, dual solutions exist within the shrinking/stretching surface. Therefore, stability analysis is required to ensure both solutions have the correct physical sense. By referring to Merkin [49] and Weidman [50], we start the stability analysis with consideration of the unsteady form of the momentum and energy equations as follows:

$$\frac{\partial u}{\partial t} + u\frac{\partial u}{\partial x} + v\frac{\partial u}{\partial y} = \frac{\mu_{hnf}}{\rho_{hnf}}\frac{\partial^2 u}{\partial y^2}, \tag{11}$$

$$\frac{\partial T}{\partial t} + u\frac{\partial T}{\partial x} + v\frac{\partial T}{\partial y} = \alpha_{hnf}\frac{\partial^2 T}{\partial y^2} + \frac{\mu_{hnf}}{(\rho C_p)_{hnf}}\left(\frac{\partial u}{\partial y}\right)^2. \tag{12}$$

We also implement a new dimensionless time variable $\tau$ in the following similarity variables:

$$u = ax\frac{\partial f}{\partial \eta}(\eta,\tau), \qquad v = -\sqrt{av_f}\,f(\eta,\tau),$$

$$\theta(\eta,\tau) = \frac{T - T_\infty}{T_w - T_\infty}, \qquad \eta = \sqrt{\frac{a}{v_f}}\,y, \qquad \tau = at. \tag{13}$$

Then with the usage of equation (13), equations (11) and (12) turn out to be

$$\frac{\mu_{hnf}/\mu_f}{\rho_{hnf}/\rho_f}\frac{\partial^3 f}{\partial \eta^3} + f\frac{\partial^2 f}{\partial \eta^2} - \left(\frac{\partial f}{\partial \eta}\right)^2 - \frac{\partial^2 f}{\partial \eta \partial \tau} = 0, \tag{14}$$

$$\frac{k_{hnf}/k_f}{\Pr\left(\rho C_p\right)_{hnf}/(\rho C_p)_f}\frac{\partial^2 \theta}{\partial \eta^2} + f\frac{\partial \theta}{\partial \eta} + \frac{Ec}{(1-\phi_1)^{2.5}(1-\phi_2)^{2.5}\left(\rho C_p\right)_{hnf}/(\rho C_p)_f}\left(\frac{\partial^2 f}{\partial \eta^2}\right)^2 - \frac{\partial \theta}{\partial \tau} = 0 \tag{15}$$

and the boundary conditions (8) turn into

$$f(0,\tau)=s, \quad \frac{\partial f}{\partial \eta}(0,\tau)=\lambda \qquad \frac{\partial \theta}{\partial \eta}(0,\tau)=-\frac{k_f}{k_{hnf}}\Gamma\left(1-\theta(0,\tau)\right),$$

$$\frac{\partial f}{\partial \eta}(\eta,\tau)\to 0, \qquad \theta(\eta,\tau)\to 0 \quad \text{as} \quad \eta\to\infty. \tag{16}$$

Further, we determine the stability behavior of both solutions by using the following representations:

$$f(\eta,\tau)=f_0(\eta)+e^{-\gamma\tau}F(\eta), \qquad \theta(\eta,\tau)=\theta_0(\eta)+e^{-\gamma\tau}G(\eta) \tag{17}$$

where $F(\eta)$ and $G(\eta)$ are relatively small to $f_0(\eta)$ and $\theta_0(\eta)$, respectively. Here, $\gamma$ is the unknown eigenvalue parameter. Then, the substitution of equation (17) into equation (14) – (16) produces the following linearized equations:

$$\frac{\mu_{hnf}/\mu_f}{\rho_{hnf}/\rho_f}F'''+f_0F''+Ff_0''-2f_0'F'+\gamma F'=0, \tag{18}$$

$$\frac{k_{hnf}/k_f}{\Pr\left(\rho C_p\right)_{hnf}/\left(\rho C_p\right)_f}G''+f_0G'+F\theta_0'+\frac{Ec}{\left(1-\phi_1\right)^{2.5}\left(1-\phi_2\right)^{2.5}\left(\rho C_p\right)_{hnf}/\left(\rho C_p\right)_f}\left(2f_0''F''\right)+\gamma G=0 \tag{19}$$

correspond to the boundary conditions

$$F(0)=0, \quad F'(0)=0, \quad G'(0)=\frac{k_f}{k_{hnf}}\Gamma G(0),$$

$$F'(\infty)\to 0, \qquad G(\infty)\to 0. \tag{20}$$

After that, a normalizing boundary condition $F''(0)=1$ is used to replace $F'(\infty)\to 0$. This method also has been implemented by Harris et al. [51], Naganthran et al. [52] and Jamaludin et al. [24] to find the infinite range of eigenvalues $\gamma_1 < \gamma_2 < \gamma_3 < ...$ where the stabilizing property of the solution can be decided by the smallest eigenvalue $\gamma_1$.

## RESULTS AND DISCUSSION

In this study, equations (6) – (8) are numerically solved by using the finite difference code (bvp4c) in Matlab. The programming code is executed with the relative error tolerance of $10^{-5}$. The dual solutions were obtained by setting different initial guesses for the values of $f''(0), g''(0)$ and $\theta'(0)$ in which all the profiles must satisfy the conditions (8) asymptotically. This study is conducted with $\phi_1$ denotes the volume fraction of Cu nanoparticles and $\phi_2$ represents the volume fraction of Ag nanoparticles. Since the base fluid is water, thus the value of Prandtl number is set to 6.2 which is in accordance with room temperature of nearly 295.15K.

The accuracy of the numerical results has been validated through comparison with the previous studies. As depicted in Table 4, the values of the reduced Nusselt number $-\theta'(0)$ in the present study similar with those obtained by Gorla and Sidawi [53] and Khan and Pop [54] which were generated by using the shooting method and implicit finite difference method, respectively. Therefore, this proves that the numerical results produced by the bvp4c function are as precise as the other methods. In addition, we also compare the present result with Waini et al. [43] who also used the bvp4c function to ensure that the constructed algorithms and programming code in this study are correct and highly accurate. Besides, the result in Table 4 also clarifies that the higher values of Pradtl number enhances the rate of heat transfer.

**Table 4.** The comparison of the reduced Nusselt number $-\theta'(0)$ for $\lambda=1$, $\Gamma\to\infty$ and $s=Ec=\phi_1=\phi_2=0$.

| Pr | Gorla and Sidawi [53] | Khan and Pop [54] | Waini et al. [43] | Present |
|---|---|---|---|---|
| 0.20 | 0.16912 | 0.1691 | | 0.169090 |
| 2.00 | 0.91142 | 0.9113 | 0.911357 | 0.911358 |
| 6.13 | | | 1.759682 | 1.759685 |
| 6.20 | | | | 1.770948 |
| 7.00 | 1.89046 | 1.8954 | 1.895400 | 1.895403 |
| 7.38 | | | | 1.952017 |
| 20.00 | 3.35391 | | 3.353893 | 3.353905 |
| 21.00 | | | | 3.442071 |
| 70.00 | 6.4622 | 6.4621 | | 6.462200 |

Dual solutions exist when the sheet is stretched $(\lambda > 0)$ and also in the shrinking sheet $(\lambda < 0)$. However, there is a unique solution at the critical point $\lambda_c$ and no solution can be found when $\lambda < \lambda_c$. It means that the boundary layer separation occurs when $\lambda < \lambda_c$. The smallest eigenvalue $\gamma_1$ indicates the stability characteristic of the dual solutions. The negative value of $\gamma_1$ is specifying the development of disturbances in the solution, and hence showing that the solution is unstable. On the contrary, the solution is complying the stabilizing property when $\gamma_1$ is positive. Therefore, since Table 5 shows the result of $\gamma_1$ is positive for the first solution and negative for the second solution, thus the first solution is stable while the second solution is unstable.

**Table 5.** Smallest eigenvalue $\gamma_1$ for $\lambda \to \lambda_c$.

| $\lambda$ | $\gamma_1$ (1st Solution) | $\gamma_1$ (2nd Solution) |
|---|---|---|
| -5 | 1.6556 | -2.0185 |
| -5.7 | 0.8398 | -0.7859 |
| -5.78 | 0.2165 | -0.2130 |
| -5.785 | 0.0837 | -0.0833 |
| -5.7859 | 0.0266 | -0.0267 |

Viscous dissipation effect which represented by the Eckert number has been included in the energy equation (7). Obviously, viscous dissipation is highly related to the conversion process of kinetic energy to the internal heat energy. Figure 2 illustrates that the increment of Eckert number enhances the temperature profile. This means the viscous dissipation affects the thickness of the thermal boundary layer. The higher viscous dissipation aggravates the thermal boundary layer thickness due to the occurrence of frictional heating and thermal reversal adjacent to the surface [55]. Nusselt number is the physical quantity that represents the rate of heat transfer. As depicted in Figure 3, the Nusselt number decreases with a rise in $Ec$. It is worth mentioning that the negative sign of the Nusselt number means a reversal in the direction of heat transfer on the surface. Physically, as the viscous dissipation increases, the internal heat energy also increases which leading to the deterioration of the process of heat transfer.

Figure 4(a) shows the influence of Biot number, $\Gamma$ on the temperature profile without the presence of viscous dissipation $(Ec = 0)$ while Figure 4(b) portrays the effect of Biot number when $Ec = 1$. In Figure 4(a), an increase of $\Gamma$ contributes to the higher thermal boundary layer thickness. On the other hand, Figure 4(b) shows a decreasing trend of the thermal boundary layer thickness since the presence of viscous dissipation causes the thermal reversal. However, the surface temperature shown in Figure 4(b) is higher compared to the Figure 4(a). Figure 5 shows the dual solutions in temperature profile for some values of Biot number. As we can see the thermal boundary layer thickness lessen for both solutions. Biot number is inversely proportional the thermal resistance since it has direct proportionality to the heat transfer coefficient $h_f$. Therefore, the heat resistance declines when $\Gamma$ getting higher, which consequently increases the surface heat transfer. This is in accordance with the results shown in Figure 6 where $Nu_x \operatorname{Re}_x^{-1/2}$ is increasing with an increase in $\Gamma$. The value of critical point $\lambda_c$ remain the same in Figures 3 and 6 which means that the variances in the Eckert number and Biot number have no effect to $\lambda_c$.
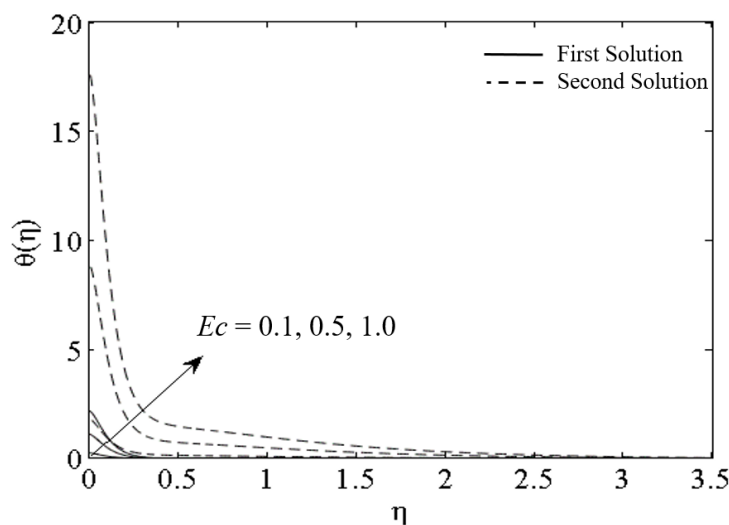


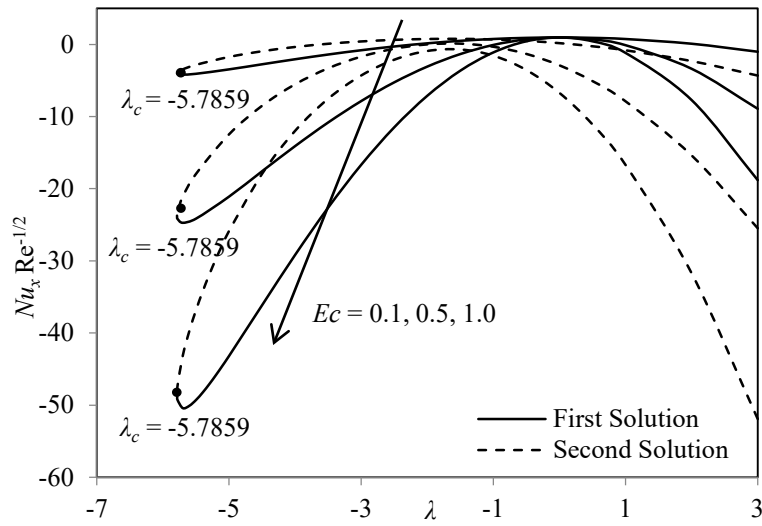**Figure 2.** The influence of viscous dissipation on $\theta(\eta)$.

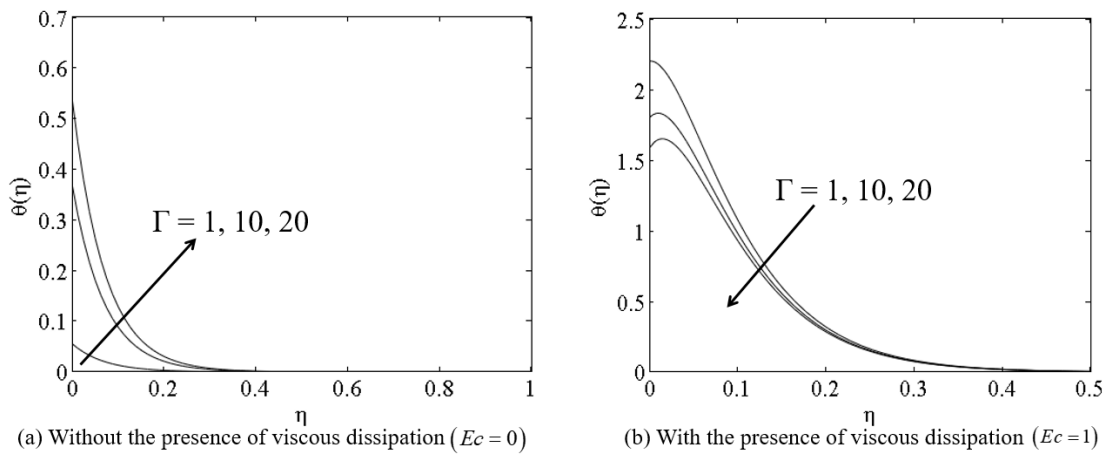**Figure 3.** Variations of $Nu_x \, \mathrm{Re}_x^{-1/2}$ with $\lambda$ for some values of $Ec$

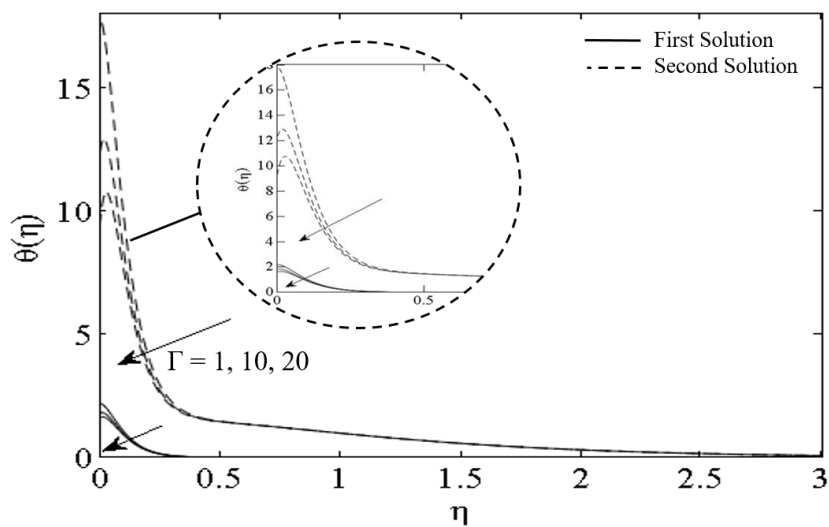**Figure 4.** The influence of Biot number on $\theta(\eta)$ without and with the presence of viscous dissipation

(a) Without the presence of viscous dissipation $(Ec = 0)$

(b) With the presence of viscous dissipation $(Ec = 1)$

**Figure 5.** Dual solutions in temperature profile for some values of Biot number when $s = 2.25$, $\mathrm{Pr} = 6.2$, $Ec = 1.0$, $\lambda = 1.0$, $\phi_1 = 0.02$ and $\phi_2 = 0.04$.
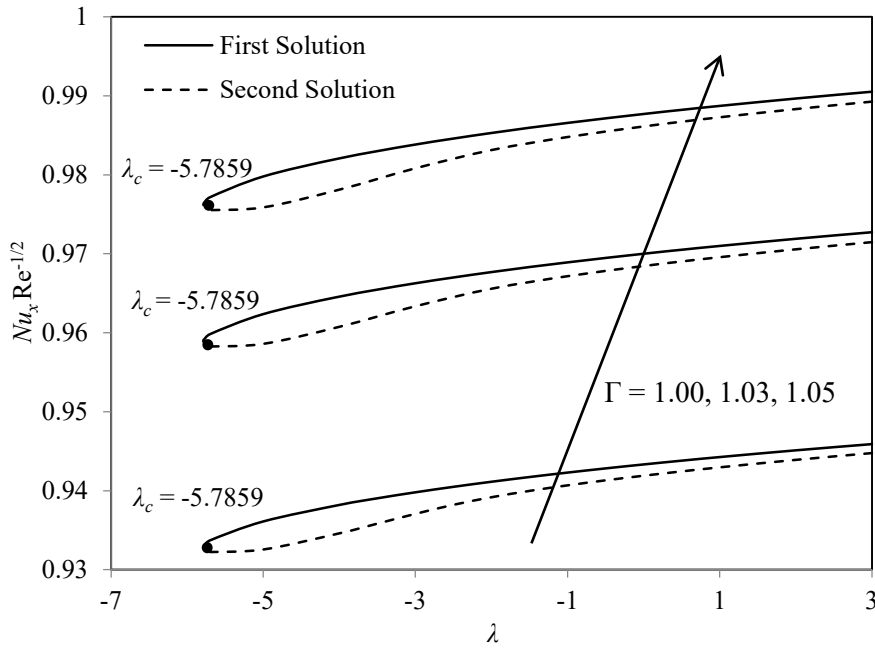
**Figure 6.** Variations of $Nu_x \, Re_x^{-1/2}$ with $\lambda$ for some values of $\Gamma$

The surface becomes permeable with the existence of suction. Therefore, suction gives a prominent impact to the velocity profile and the skin friction coefficient. Figure 7 shows that the increasing values of suction reduces the momentum boundary layer thickness. This is owing to the fact that suction acts as a deceleration factor for the fluid flow and deploys a drag force. This statement is also reflected by the results shown in Figure 8 where the magnitude of the skin friction coefficient $\left| f''(0) \right|$ increases with a rise in the suction parameter. Besides, the critical point $\lambda_c$ is getting larger as the suction increases which shows that the boundary layer separation is retarded.

In addition, different types of nanoparticles and variations of the nanoparticles concentration also affect the temperature profiles of the hybrid nanofluid. Figure 9 depicts that the increment of Cu nanoparticles concentration increases the thermal boundary layer thickness. In contrast, a different trend is shown in Figure 10 when the Ag nanoparticles concentration increases. Since the thermal boundary layer thickness reduces, thus the process of heat transfer will be easier. The results are in accordance with the listed values of the Nusselt number in Table 6. It is obviously seen that the values of $Nu_x \, Re^{-1/2}$ are lessening when the Cu nanoparticles getting concentrated. However, as the volume fraction of Ag nanoparticle increases, the values of $Nu_x \, Re^{-1/2}$ are increasing which shows that the higher concentration of Ag nanoparticles enhances the heat transfer rate of the hybrid nanofluid. Perhaps this is due to the fact that the thermal conductivity of silver is higher compared to the copper. The insertion of suction also believed to be the causal factor of such results.
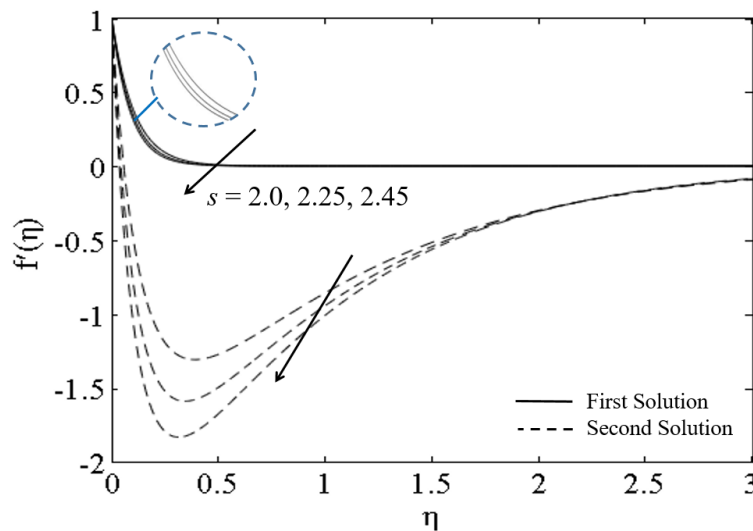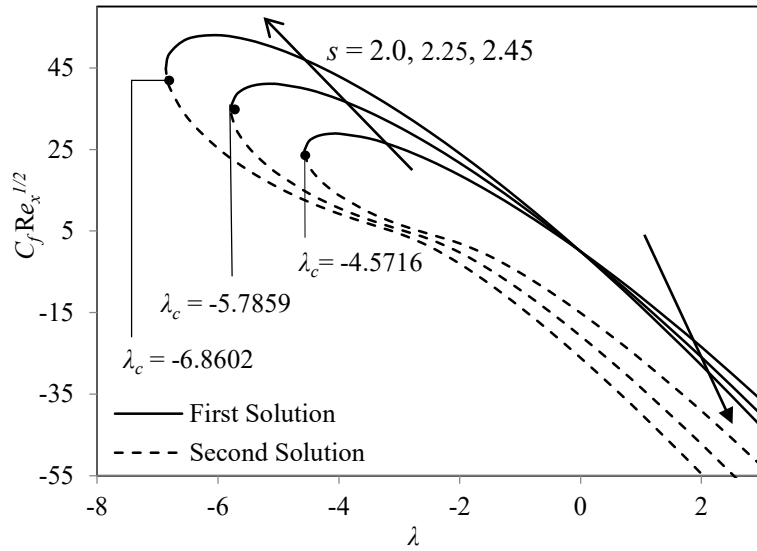


**Figure 7.** The influence of suction on $f'(\eta)$

**Figure 8.** Variations of $C_f\sqrt{Re_x}$ with $\lambda$ for some values of $s$
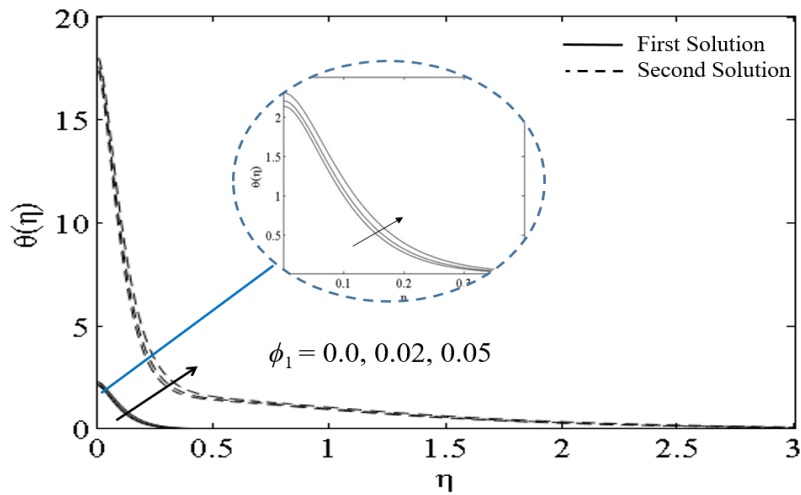


**Figure 9.** The influence of variations in Cu nanoparticles concentration on $\theta(\eta)$.
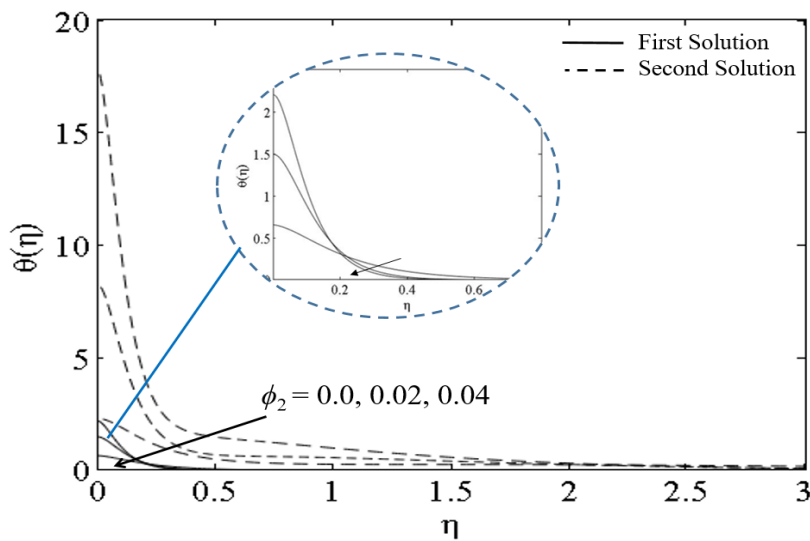


**Figure 10.** The influence of variations in Ag nanoparticles concentration on $\theta(\eta)$.

**Table 6.** The comparison of $Nu_x \, Re^{-1/2}$ with variations in $\phi_1$ (Cu nanoparticles) and $\phi_2$ (Ag nanoparticles) when $s = 2.25$, $Ec = 0$, $Pr = 6.2$, $\lambda = 1$ and $\Gamma \to \infty$.

| $\phi_1$ | Ag-Cu/Water $(\phi_2 = 0.02)$ | $\phi_2$ | Ag-Cu/Water $(\phi_1 = 0.02)$ |
|---|---|---|---|
| 0.02 | 15.59855 | 0.02 | 15.59855 |
| 0.05 | 15.54594 | 0.05 | 17.62359 |
| 0.07 | 15.51140 | 0.07 | 18.98622 |
| 0.1 | 15.46054 | 0.1 | 21.04027 |

Figure 11 elucidates the impact of different base fluid used in the hybrid nanofluid to the temperature profiles. Thermal boundary layer thickness in the flow of Ag-Cu/kerosene hybrid nanofluid is the lowest, followed by Ag-Cu/methanol and Ag-Cu/water. Indirectly, the heat transfer process involving the kerosene is better than methanol and water. This is also related to the higher value of Prandtl number for kerosene as depicted in Table 3. Since the thermal diffusivity is lower when the value of Prandtl number increases, thus the rate of heat transfer will be escalated. This result is also in an excellent agreement with Reddy et al. [48] where they concluded kerosene exhibited a tremandous heat transfer performance. Therefore, the use of kerosene as the base fluid in the hybrid nanofluid can be commercialized for various industrial sector.
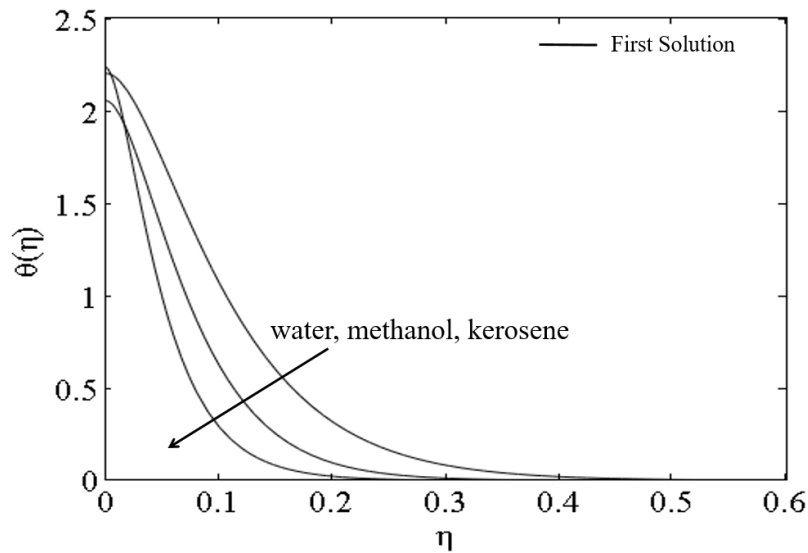


**Figure 11.** The influence of different types of base fluids on $\theta(\eta)$.

## CONCLUSION

This study scrutinized the flow and heat transfer of Ag-Cu hybrid nanofluid with consideration of suction, viscous dissipation and convective boundary condition. Dual solutions were obtained for a certain range of stretching/shrinking parameter. From the stability analysis, the first solution is stable since the generated smallest eigenvalue is positive. The variations of Eckert number and Biot number gave different impact to the rate of heat transfer. Conclusively, the heat transfer rate enhanced with a rise in the Biot number but deteriorated with an increase in the viscous dissipation. Higher volume fraction of Ag nanoparticles also contributed to the higher rate of heat transfer. The existence of suction affected the flow of the Ag-Cu hybrid nanofluid and increased the skin friction coefficient. Besides, the momentum boundary layer was thickening as the viscous dissipation and Cu nanoparticles concentration increased. A better heat transfer performance can be achieved with the use of kerosene as the base fluid. The advantage of the employed model will help the engineers to optimize the utilization of Ag-Cu hybrid nanofluid as a propitious cooling medium in the various industrial sector.

## ACKNOWLEDGEMENT

## REFERENCES

[1]  S. U. S. Choi and J. A. Eastman, "Enhancing thermal conductivity of fluids with nanoparticles," in *The Proceedings of the 1995 ASME International Mechanical Engineering Congress and Exposition*, 1995, vol. 231, pp. 99–105.

[2]  R. Saidur, K. Y. Leong, and H. A. Mohammad, "A review on applications and challenges of nanofluids," *Renew. Sustain. Energy Rev.*, vol. 15, no. 3, pp. 1646–1668, 2011.

[3]  C. T. Nguyen, G. Roy, C. Gauthier, and N. Galanis, "Heat transfer enhancement using Al$_2$O$_3$-water nanofluid for an electronic liquid cooling system," *Appl. Therm. Eng.*, vol. 27, pp. 1501–1506, 2007.

[4]  M. Khoshvaght-Aliabadi and A. Alizadeh, "An experimental study of Cu-water nanofluid flow inside serpentine tubes with variable straight-section lengths," *Exp. Therm. Fluid Sci.*, vol. 61, no. February, pp. 1–11, 2015.

[5]  H. D. Koca, S. Doganay, and A. Turgut, "Thermal characteristics and performance of Ag-water nanofluid: Application to natural circulation loops," *Energy Convers. Manag.*, vol. 135, pp. 9–20, 2017.

[6]  K. V. Wong and O. De Leon, "Applications of nanofluids: Current and future," *Adv. Mech. Eng.*, vol. 2010, pp. 1–11, 2010.

[7]  O. Manca, Y. Jaluria, and D. Paulikakos, "Heat transfer in nanofluids," *Adv. Mech. Eng.*, vol. 380826, pp. 3–19, 2010.

[8]  K. H. Solangi *et al.*, "A comprehensive review of thermo-physical properties and convective heat transfer to nanofluids," *Energy*, vol. 89, pp. 1065–1086, 2015.

[9]  R. Thaker and J. Patel, "Application of nanofluids in solar energy," *J. Altern. Energy Sources Technol.*, vol. 6, no. 2, pp. 1–11, 2016.

[10] A. M. Rohni, S. Ahmad, and I. Pop, "Flow and heat transfer over an unsteady shrinking sheet with suction in a nanofluid using Buongiorno's model," *Int. Commun. Heat Mass Transf.*, vol. 43, no. 7–8, pp. 75–80, 2013.

[11] S. Mansur and A. Ishak, "The flow and heat transfer of a nanofluid past a stretching/shrinking sheet with a convective boundary condition," *Abstr. Appl. Anal.*, vol. 2013, p. 350647, 2013.

[12] D. Pal and G. Mandal, "Hydromagnetic convective-radiative boundary layer flow of nanofluids induced by a non-linear vertical stretching/shrinking sheet with viscous-Ohmic dissipation," *Powder Technol.*, vol. 279, pp. 61–74, 2015.

[13] M. Awais, T. Hayat, S. Irum, and A. Alsaedi, "Heat generation/absorption effects in a boundary layer stretched flow of Maxwell nanofluid : Analytic and numeric Solutions," *PLoS One*, vol. 10(6), no. e0129814, pp. 1–18, 2015.

[14] T. Hayat, M. Imtiaz, and A. Alsaedi, "Magnetohydrodynamic stagnation point flow of a Jeffrey nanofluid with Newtonian heating," *J. Aerosp. Eng.*, vol. 29, no. 3, p. 04015063, 2016.

[15] G. Bal Reddy, B. Shankar Goud, and M. N. Raja Shekar, "Keller box solution of magnetohydrodynamic boundary layer flow of nanofluid over an exponentially stretching permeable sheet," *Int. J. Mech. Eng. Technol.*, vol. 9, no. 10, pp. 1646–1656, 2018.

[16] K. Rafique *et al.*, "Numerical solution of Casson nanofluid flow over a non-linear inclined surface with Soret and Dufour effects by Keller-Box method," *Front. Phys.*, vol. 7, pp. 1–13, 2019.

[17] J. Sarkar, P. Ghosh, and A. Adil, "A review on hybrid nanofluids: Recent research, development and applications," *Renew. Sustain. Energy Rev.*, vol. 43, pp. 164–177, 2015.

[18] S. P. A. Devi and S. S. U. Devi, "Numerical investigation of hydromagnetic hybrid Cu - Al$_2$O$_3$/water nanofluid flow over a permeable stretching sheet with suction," *Int. J. Nonlinear Sci. Numer. Simul.*, vol. 17, no. 5, pp. 249–257, 2016.

[19] A. A. Minea, "Hybrid nanofluids based on Al$_2$O$_3$, TiO$_2$ and SiO$_2$: Numerical evaluation of different approaches," *Int. J. Heat Mass Transf.*, vol. 104, pp. 852–860, 2017.

[20] T. Hayat, S. Nadeem, and A. U. Khan, "Rotating flow of Ag-CuO/H$_2$O hybrid nanofluid with radiation and partial slip boundary effects," *Eur. Phys. J. E*, vol. 41, no. 6, 2018.

[21] I. Waini, A. Ishak, and I. Pop, "Hybrid nanofluid flow past a permeable moving thin needle," *Mathematics*, vol. 8, no. 4, pp. 612–629, 2020.

[22] N. S. Khashi'ie, N. M. Arifin, E. H. Hafidzuddin, and N. Wahi, "Thermally stratified flow of Cu-Al$_2$O$_3$/water hybrid nanofluid past a permeable stretching/ shrinking circular cylinder," *J. Adv. Res. Fluid Mech. Therm. Sci.*, vol. 63, no. 1, pp. 154–163, 2019.

[23] N. A. Zainal, R. Nazar, K. Naganthran, and I. Pop, "Unsteady three-dimensional MHD non-axisymmetric homann stagnation point flow of a hybrid nanofluid with stability analysis," *Mathematics*, vol. 8, no. 5, 2020.

[24] A. Jamaludin, K. Naganthran, R. Nazar, and I. Pop, "MHD mixed convection stagnation-point flow of Cu-Al$_2$O$_3$/water hybrid nanofluid over a permeable stretching/shrinking surface with heat source/sink," *Eur. J. Mech. /B Fluids*, vol. 84, pp. 71–80, 2020.

[25] M. Yousefi, S. Dinarvand, M. Eftekhari Yazdi, and I. Pop, "Stagnation-point flow of an aqueous titania-copper hybrid nanofluid toward a wavy cylinder," *Int. J. Numer. Methods Heat Fluid Flow*, vol. 28, no. 7, pp. 1716–1735, 2018.

[26] S. Dinarvand, "Nodal/saddle stagnation-point boundary layer flow of CuO–Ag/water hybrid nanofluid: A novel hybridity model," *Microsyst. Technol.*, vol. 25, no. 7, pp. 2609–2623, 2019.

[27] H. Shojaie Chahregh and S. Dinarvand, "TiO$_2$-Ag/blood hybrid nanofluid flow through an artery with applications of drug delivery and blood circulation in the respiratory system," *Int. J. Numer. Methods Heat Fluid Flow*, vol. 3, no. 11, pp. 4775–4796, 2020.

[28] X. Zhang and J. Ouyang, "Meshless analysis of heat transfer due to viscous dissipation in polymer flow," *Eng. Anal. with Bound. Elem.*, vol. 32, pp. 41–51, 2008.

[29] R. Sharma, R. Bhargava, and I. V Singh, "Combined effect of magnetic field and heat absorption on unsteady free convection and heat transfer flow in a micropolar fluid past a semi-infinite moving plate with viscous dissipation using element free Galerkin method," *Appl. Math. Comput.*, vol. 217, pp. 308–321, 2010.

[30] R. C. Bataller, "Viscoelastic fluid flow and heat transfer over a stretching sheet under the effects of a non-uniform heat source, viscous dissipation and thermal radiation," *Int. J. Heat Mass Transf.*, vol. 50, pp. 3152–3162, 2007.

[31] F. Mabood, W. A. Khan, and A. I. M. Ismail, "MHD boundary layer flow and heat transfer of nanofluids over a nonlinear stretching sheet: A numerical study," *J. Magn. Magn. Mater.*, vol. 374, pp. 569–576, 2015.

[32] M. H. Yazdi, S. Abdullah, I. Hashim, and K. Sopian, "Effects of viscous dissipation on the slip MHD flow and heat transfer past a permeable surface with convective boundary conditions," *Energies*, vol. 4, no. 12, pp. 2273–2294, 2011.

[33] R. Dhanai, P. Rana, and L. Kumar, "Multiple solutions of MHD boundary layer flow and heat transfer behavior of nanofluids

induced by a power-law stretching/shrinking permeable sheet with viscous dissipation," *Powder Technol.*, vol. 273, pp. 62–70, 2015.

[34] M. M. Nandeppanavar, M. S. Abel, and K. Vajravelu, "Flow and heat transfer characteristics of a viscoelastic fluid in a porous medium over an impermeable stretching sheet with viscous dissipation," *Int. J. Heat Mass Transf.*, vol. 53, pp. 4707–4713, 2010.

[35] V. M. Soundalgekar, "Viscous dissipation effects on unsteady free convective flow past in infinite, vertical porous plate with constant suction," *Int. J. Heat Mass Transf.*, vol. 15, pp. 1253–1261, 1972.

[36] L. A. Lund, Z. Omar, I. Khan, A. H. Seikh, E.-S. M. Sherif, and K. S. Nisar, "Stability analysis and multiple solution of Cu-$Al_2O_3$/$H_2O$ nanofluid contains hybrid nanomaterials over a shrinking surface in the presence of viscous dissipation," *J. Mater. Res. Technol.*, vol. 9, no. 1, pp. 421–432, 2020.

[37] H. M. Sayed, E. H. Aly, and K. Vajravelu, "Influence of slip and convective boundary conditions on peristaltic transport of non-Newtonian nanofluids in an inclined asymmetric channel," *Alexandria Eng. J.*, vol. 55, no. 3, pp. 2209–2220, 2016.

[38] R. Malik, M. Khan, A. Munir, and W. A. Khan, "Flow and heat transfer in Sisko fluid with convective boundary condition," *PLoS One*, vol. 9, no. 10, p. e107989, 2014.

[39] W. Ibrahim and R. Ul Haq, "Magnetohydrodynamic (MHD) stagnation point flow of nanofluid past a stretching sheet with convective boundary condition," *J. Brazilian Soc. Mech. Sci. Eng.*, vol. 38, no. 4, pp. 1155–1164, 2016.

[40] H. Rosali, A. Ishak, R. Nazar, and I. Pop, "Mixed convection boundary layer flow past a vertical cone embedded in a porous medium subjected to a convective boundary condition," *Propuls. Power Res.*, vol. 5, no. 2, pp. 2–6, 2016.

[41] A. Moghadassi, E. Ghomi, and F. Parvizian, "A numerical study of water based $Al_2O_3$ and $Al_2O_3$-Cu hybrid nanofluid effect on forced convective heat transfer," *Int. J. Therm. Sci.*, vol. 92, pp. 50–57, 2015.

[42] S. S. U. Devi and S. P. A. Devi, "Numerical investigation of three-dimensional hybrid Cu-$Al_2O_3$/water nanofluid flow over a stretching sheet with effecting Lorentz force subject to Newtonian heating," *Can. J. Phys.*, vol. 94, no. 5, pp. 490–496, 2016.

[43] I. Waini, A. Ishak, and I. Pop, "Hybrid nanofluid flow and heat transfer past a permeable stretching/shrinking surface with a convective boundary condition," *J. Phys. Conf. Ser.*, vol. 1366, no. 1, 2019.

[44] E. Abu-nada, "Application of nanofluids for heat transfer enhancement of separated flows encountered in a backward facing step," *Int. J. Heat Fluid Flow*, vol. 29, pp. 242–249, 2008.

[45] R. Jusoh, R. Nazar, and I. Pop, "Magnetohydrodynamic boundary layer flow and heat transfer of nanofluids past a bidirectional exponential permeable stretching / shrinking sheet with viscous dissipation effect," *ASME J. Heat Transf.*, vol. 141, no. 1, p. 012406, 2019.

[46] G. Aaiza, I. Khan, and S. Shafie, "Energy transfer in mixed convection MHD flow of nanofluid containing different shapes of nanoparticles in a channel filled with saturated porous medium," *Nanoscale Res. Lett.*, vol. 10, no. 490, pp. 1–14, 2015.

[47] R. Jusoh, R. Nazar, and I. Pop, "Impact of heat generation/absorption on the unsteady magnetohydrodynamic stagnation point flow and heat transfer of nanofluids," *Int. J. Numer. Methods Heat Fluid Flow*, vol. 30, no. 2, pp. 557–574, 2019.

[48] J. V. Ramana Reddy, V. Sugunamma, and N. Sandeep, "Impact of nonlinear radiation on 3D magnetohydrodynamic flow of methanol and kerosene based ferrofluids with temperature dependent viscosity," *J. Mol. Liq.*, vol. 236, pp. 93–100, 2017.

[49] J. H. Merkin, "Mixed convection boundary layer flow on a vertical surface in a saturated porous medium," *J. Eng. Math.*, vol. 14, no. 4, pp. 301–313, 1980.

[50] P. D. Weidman, D. G. Kubitschek, and A. M. J. Davis, "The effect of transpiration on self-similar boundary layer flow over moving surfaces," *Int. J. Eng. Sci.*, vol. 44, no. 11–12, pp. 730–737, 2006.

[51] S. D. Harris, D. B. Ingham, and I. Pop, "Mixed convection boundary-layer flow near the stagnation point on a vertical surface in a porous medium: Brinkman model with slip," *Transp. Porous Media*, vol. 77, no. 2, pp. 267–285, 2009.

[52] I. Pop, K. Naganthran, R. Nazar, and A. Ishak, "The effect of vertical throughflow on the boundary layer of a nanofluid past a stretching/shrinking sheet: A revised model," *Int. J. Numer. Methods Heat Fluid Flow*, vol. 27, no. 9, pp. 1910–1927, 2016.

[53] R. S. Reddy Gorla and I. Sidawi, "Free convection on a vertical stretching surface with suction and blowing," *Appl. Sci. Res.*, vol. 52, no. 3, pp. 247–257, 1994.

[54] W. A. Khan and I. Pop, "Boundary-layer flow of a nanofluid past a stretching sheet," *Int. J. Heat Mass Transf.*, vol. 53, no. 11–12, pp. 2477–2483, 2010.

[55] K. Ali, M. Ashraf, S. Ahmad, and K. Batool, "Viscous dissipation and radiation effects in MHD stagnation point flow towards a stretching sheet with induced magnetic field," *World Appl. Sci. J.*, vol. 16, no. 11, pp. 1638–1648, 2012.